Journal of Coordination Chemistry

ISSN: 0095-8972 (Print) 1029-0389 (Online) Journal homepage: http://www.tandfonline.com/loi/gcoo20

Mixed ligand Cu(II) complexes containing o-vanillin-l-tryptophan Schiff base and heterocyclic nitrogen bases: synthesis, structural characterization, and biological properties

L. Subha, C. Balakrishnan, S. Thalamuthu & M.A. Neelakantan

To cite this article: L. Subha, C. Balakrishnan, S. Thalamuthu & M.A. Neelakantan (2015) Mixed ligand Cu(II) complexes containing o-vanillin-l-tryptophan Schiff base and heterocyclic nitrogen bases: synthesis, structural characterization, and biological properties, Journal of Coordination Chemistry, 68:6, 1021-1039, DOI: 10.1080/00958972.2015.1008466

To link to this article: http://dx.doi.org/10.1080/00958972.2015.1008466

View supplementary material

Accepted author version posted online: 19 Jan 2015.
Published online: 11 Feb 2015.

Submit your article to this journal

Article views: 133

View related articles

View Crossmark data

Citing articles: 5 View citing articles

Full Terms & Conditions of access and use can be found at
http://www.tandfonline.com/action/journalInformation?journalCode=gcoo20

Download by: [Mizoram University] **Date:** 28 December 2015, At: 14:52

Journal of Coordination Chemistry, 2015
Vol. 68, No. 6, 1021–1039, http://dx.doi.org/10.1080/00958972.2015.1008466

Taylor & Francis
Taylor & Francis Group

Downloaded by [Mizoram University] at 14:52 28 December 2015

Mixed ligand Cu(II) complexes containing *o*-vanillin-L-tryptophan Schiff base and heterocyclic nitrogen bases: synthesis, structural characterization, and biological properties

L. SUBHA, C. BALAKRISHNAN, S. THALAMUTHU and M.A. NEELAKANTAN*

Chemistry Research Centre, National Engineering College, Kovilpatti, India

(*Received 15 September 2014; accepted 30 December 2014*)

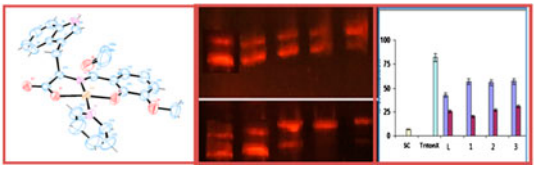

[Cu(L)] (**1**) and mixed ligand copper(II) complexes [Cu(L)(A)] (**2** and **3**), where **L** is the Schiff base derived from *o*-vanillin and L-tryptophan and **A** is pyridine (**2**) and imidazole (**3**), were synthesized and characterized using conventional and spectral techniques. **2** was structurally characterized using single crystal X-ray crystallography showing that Cu(II) is coordinated through N_2O_2 donors in a square plane. The EPR spectra of the complexes in frozen solution support a square-based structure. Electrochemical behavior of the complexes has been studied by cyclic voltammetry. The DNA-binding properties of **L** and **1–3** with calf thymus DNA were investigated by spectral and kinetic methods. For all the complexes, the maximum value of binding constant (0.38×10^6) was achieved with **3** by spectroscopic titration. The ability of compounds to break pUC19 DNA was checked by gel electrophoresis. The ligand and copper complexes exert cytotoxicity against MCF-7 cell line.

Keywords: Copper(II) complex; Amino acid Schiff base; Crystal structure; Spectroscopy; DNA binding and cleavage

1. Introduction

The design and development of new DNA-binding transition metal complexes is an active area of research because of their potential use as drugs [1–3]. Transition metal complexes with their electronic and structural diversities can interact with DNA through ionic binding, covalent modification, intercalation, and major/minor groove binding [4, 5]. Metal complex–DNA interactions have effects on reactions involving free-radicals. The scavenging of

*Corresponding author. Emails: drmaneelakantan@gmail.com, maneels@rediffmail.com

© 2015 Taylor & Francis

superoxide and hydroxyl radicals causes DNA mutation and leads to diseases like cancer, liver malfunction, and cardiovascular problems [6, 7]. Platinum-based drugs are the only DNA-targeted metal containing drugs in clinical use [8]. There has been considerable interest in the development of new metal-based drugs with higher efficacy, lesser side effects, and low clinical costs. In addition to platinum, several metals are currently being investigated for their anticancer activity [9, 10]. Copper complexes have been studied extensively because of their biologically accessible redox potential and their relatively high affinity for nucleobases. Copper complexes have the potential to cleave DNA both oxidatively [11] and hydrolytically [12]. Recent studies of copper complexes have focused on the binding of copper complexes with DNA [13–16]. Synthesis of biologically important amino acid-based transition metal complexes which are capable of cleaving DNA attracted much attention [17–20]. Cu(II) complexes of tryptophan-based Schiff bases strongly bind with DNA and cleave it [21]. Mixed ligand copper(II)-Schiff base-heterocyclic base complexes show strong DNA binding, cleavage, and exhibit cytotoxic activities [22, 23].

Therefore, with our ongoing interest in mixed ligand complexes [24–26], we focus on the development of copper(II) complexes containing amino acid Schiff bases and monodentate heterocyclic nitrogen base co-ligands. The present work consists of synthesis and characterization of binary and mixed ligand Cu(II) complexes containing *o*-vanillin-L-tryptophan Schiff base (**L**) and pyridine/imidazole as co-ligands. The complexes were characterized by microanalytical, spectroscopic, and single crystal X-ray diffraction studies. The electrochemical behavior of the complexes was investigated by cyclic voltammetry. We determined the binding constants (K_b) and quenching constants (K_{SV}) for the interaction of **L** and **1–3** under physiological conditions with calf thymus-DNA (CT DNA). The DNA cleaving was tested against pUC19 DNA in the absence and presence of ascorbic acid. The cytotoxicity of the compounds against MCF-7 cell line was evaluated with MTT assay.

2. Experimental

2.1. *Materials*

All reagents were purchased from commercial sources and used as received. L-tryptophan, *o*-vanillin, pyridine, imidazole, ascorbic acid, and copper(II) perchlorate hexahydrate were purchased from Sigma Aldrich, USA and used as received. Supercoiled pUC19 DNA (CsCl purified) and calf thymus (CT) DNA were purchased from Genei, Bangalore and stored at 4 °C. Tris-(hydroxymethyl)-aminomethane-HCl (Tris–HCl) and methanol were supplied by Merck, India. Tris–HCl buffer solution was prepared using triple distilled water. The solvents were dried and purified before being used according to standard methods [27].

2.2. *Characterization techniques*

CHN analyses were carried out using an Elemental Vario EL III CHNOS elemental analyzer. IR spectra were recorded on an FTIR Shimadzu 8400S spectrophotometer from 4000 to 400 cm^{-1} using KBr pellets. **L** and **1–3** were characterized by electronic spectra on a Shimadzu UV-2450 spectrophotometer. Fluorescence spectra were recorded on a Shimadzu RF-5301PC spectrofluorophotometer. Electrospray ionization mass spectra (ESI-MS) were recorded from a Thermo Finnigan LCQ 6000 advantage max ion trap mass spectrometer

Downloaded by [Mizoram University] at 14:52 28 December 2015

using acetonitrile as carrier solvent. The X-band EPR spectra of **1–3** in DMSO at room temperature and liquid nitrogen temperature were obtained on a Varian spectrometer using tetracyanoethylene (TCNE) as the "g" (2.0027) marker. CH11008 electrochemical analyzer was used to record the cyclic voltammogram. The three-electrode system consisting of a glassy carbon (working electrode), a platinum wire (auxiliary electrode), and Ag/AgCl (reference electrode) was used for all electrochemical studies. Cyclic voltammograms were recorded on a different scan rate (50–250 mV s^{-1}) at room temperature using DMSO as solvent. The supporting electrolyte used was tetrabutylammonium perchlorate (TBAP).

2.3. *Synthesis*

2.3.1. Synthesis of (E)-2-(2-hydroxy-3-methoxybenzylideneamino)-3-(1H-indol-3-yl) propanoic acid (L). To the sodium salt of L-tryptophan (0.204 g, 1 mM), methanolic solution of *o*-vanillin (0.152 g, 1 mM) was added slowly and refluxed at 60 °C for 2 h. The reaction mixture was kept at room temperature for solvent evaporation. The yellow shiny compound (**L**) was obtained and separated by filtration. The compound was washed with chloroform and dried at room temperature. The purity was checked by HPLC and ^{1}H NMR (figure S1, see online supplemental material at http://dx.doi.org/10.1080/00958972.2015.1008466). Yield: 84%. m.p.: 210 °C. Anal. Calcd for [$C_{19}H_{18}O_4N_2$]: C, 67.44; H, 5.36; N, 8.28%. Found: C, 67.83; H, 5.26; N, 7.97. FTIR (KBr, cm^{-1}) (Selected bands): 1635 ν(–CH=N–), 1223 ν(C–O), 1612 ν_{asym}(COO–), 1394 ν_{sym}(COO–). λ_{max}/nm (in DMSO)(ε/M^{-1} cm^{-1}): 422 (3370), 293 (6925), ESI-MS: *m/z* 339 $[M + H]^+$.

2.3.2. Synthesis of [Cu(L)] (1). The methanolic solution of **L** (0.339 g, 1 mM) was refluxed with $Cu(ClO_4)_2{\cdot}6H_2O$ (0.370 g, 1 mM) at 60 °C for 2 h. Complex **1** acquired by evaporation of solvent was washed with water, followed by chloroform. Finally it was dried in a vacuum desiccator over fused $CaCl_2$. Yield: 70–74%. m.p.: 300 °C. Anal. Calcd for [$CuC_{19}H_{16}N_2O_4{\cdot}CH_3OH$]: C, 55.61; H, 4.67; N, 6.49%. Found: C, 56.02; H, 4.37; N, 6.92. FTIR (KBr, cm^{-1}) (Selected bands): 1630 ν(–CH=N–), 1219 ν(C–O), 249 $\Delta\nu(COO^-)$. Electronic spectrum in DMSO solution, λ_{max}/nm (ε/M^{-1} cm^{-1}): 293 (7185), 380 (3190), 590 (84.86). ESI-MS: *m/z* 441 $[M^+]$.

Caution! Perchlorate salts of metal complexes with organic ligands are potentially explosive. They should be handled in small quantities and with caution.

2.3.3. Synthesis of [Cu(L)(A)] (2 and 3). A methanolic solution of $CuCl_2{\cdot}2H_2O$ (0.170 g, 1.0 mM) was added slowly to **L** in methanol (0.339 g, 1.0 mM) and refluxed at 60 °C for 2 h. To this reaction mixture, methanolic solution of heterocyclic base [0.079 g pyridine for **2**; 0.068 g imidazole for **3** (1.0 mM)] was added dropwise and stirred for an hour. The green precipitate obtained was separated by filtration and washed with water and then $CHCl_3$ and dried in a vacuum desiccator over fused $CaCl_2$.

For **2**, Yield: 80–83%. m.p.: 300 °C. Anal. Calcd for [$CuC_{19}H_{16}N_2O_4.C_5H_5N$]: C, 60.18; H, 4.41; N, 8.77%. Found: C, 59.97; H, 4.47; N, 8.82. FTIR (KBr, cm^{-1}) (Selected bands): 1629 ν(–CH=N–), 1217 ν(C–O), 248 $\Delta\nu(COO^-)$. Electronic spectrum in DMSO solution, λ_{max}/nm (ε/M^{-1} cm^{-1}): 298 (6870), 381 (4445), 598 (117.2). ESI-MS: *m/z* 506 $[M]^+$.

Downloaded by [Mizoram University] at 14:52 28 December 2015

For **3**, Yield: 85–89%. m.p.: 300 °C. Anal. Calcd for $[CuC_{19}H_{16}N_2O_4.C_3H_4N_2]$: C, 56.20; H, 4.56; N, 11.72. Found: C, 56.46; H, 4.31; N, 11.97%. FTIR (KBr, cm^{-1}) (Selected bands): 1628 ν(–CH=N–), 1216 ν(C–O), 250 $\Delta\nu(COO^-)$. Electronic spectrum in DMSO solution, λ_{max}/nm ($\varepsilon/M^{-1}\,cm^{-1}$): 293 (6995), 381 (4574), 607 (117.77). ESI-MS: *m/z* 468 $[M]^+$.

2.4. *Single-crystal X-ray crystallography*

The single crystal X-ray diffraction data were recorded using the ω scan method on a Bruker SMART APEX II area detector using graphite monochromated Mo Kα radiation (λ = 0.71073 Å). The unit cell parameters were determined from 36 frames (0.5° phi-scan) measured from three different crystallographic zones, using the method of difference vectors. The intensity data were collected with an average fourfold redundancy per reflection and optimum resolution (0.75 Å). The intensity data collection, frames integration, LP correction, and decay correction were done using SAINT-NT (version 6.0) software. Empirical absorption correction (multiscan) was performed using SADABS [28]. The structures were solved by direct methods using the SHELXS-97 program and refined by full-matrix least-squares of SHELXL-97 [29]. The non-hydrogen atoms were refined with anisotropic displacement parameters. All hydrogens were placed at calculated positions and refined as riding, using isotropic displacement parameters. The geometric calculations were performed by using PARST program [30]. The linear absorption coefficient for Mo Kα radiation is 0.946 mm^{-1}.

2.5. *DNA binding studies*

DNA binding of **L** and **1–3** were studied using absorption spectroscopy, fluorescence spectroscopy, and viscosity.

2.5.1. Absorption spectral studies. The interactions of metal complexes with CT-DNA were studied with absorption spectroscopy in order to investigate the possible binding mode and the binding constants (K_b) to CT-DNA. The stock solution of DNA was prepared by dissolving DNA in 5 mM Tris–HCl/50 mM NaCl (tris–HCl buffer, pH 7.2) buffer solution at room temperature. The concentration of CT-DNA was determined by recording the absorption intensity of CT-DNA in Tris–HCl buffer at 260 nm with a molar extinction coefficient of 6600 $dm^3\,M^{-1}\,cm^{-1}$. The ratio of absorbance of CT-DNA in buffer at 260 and 280 nm (A_{260}/A_{280}) of *ca.* 1.9:1 suggests the CT-DNA is free from protein. The DNA titrations were performed by keeping the concentration of the copper complex constant (20 μM) with varying DNA concentrations (from 0 to 120 μM). While measuring the absorption spectra, equal amount of DNA was added to both the complex solution and reference solution to eliminate the absorbance of DNA itself.

The binding constants of **1–3** were calculated from the absorption data using the following equation [31],

$$\frac{[DNA]}{(\varepsilon_a - \varepsilon_f)} = \frac{[DNA]}{(\varepsilon_b - \varepsilon_f)} + \frac{1}{K_b(\varepsilon_b - \varepsilon_f)} \quad (1)$$

Downloaded by [Mizoram University] at 14:52 28 December 2015

where ε_a, ε_f, and ε_b are the molar extinction coefficients of the apparent, free, and bound compounds, respectively. A plot of [DNA]/($\varepsilon_a - \varepsilon_f$) *versus* [DNA] gives slope and an intercept where the ratio of the slope and the intercept gives the binding constant (K_b).

2.5.2. Fluorescence studies (competitive binding studies). Emission intensity measurements were carried out to investigate whether **1–3** can displace EB from the CT-DNA-EB adduct in 0.005 M Tris–HCl/0.050 M NaCl buffer solution (pH = 7.2). A 1 mL solution of EB (2.5 μM) and CT DNA (10 μM) was added with different concentrations of **1–3** (0–60 μM). The fluorescence spectra at 615 nm with excitation wavelength of 543 nm were recorded at room temperature and the emission range was adjusted before measurements. The spectra were analyzed according to the classical Stern–Volmer equation [32]:

$$\frac{I_0}{I} = 1 + K_{SV}[Q] \tag{2}$$

where I_0 and I are the fluorescence intensities of EB-DNA in the absence and presence of quencher, respectively, K_{SV} is the linear Stern–Volmer quenching constant and [Q] is the concentration of the quencher. The apparent binding constant (K_{app}) was calculated using the equation $K_{app} = K_{EB}[EB]/[complex]$, where [complex] is the concentration of the complex at which there is 50% reduction in the fluorescence intensity of EB, $K_{EB} = 1.0 \times 10^7\ M^{-1}$ and [EB] = 2.5 μM.

2.5.3. Viscosity measurements. For viscosity measurements, an Ostwald-type viscometer was thermostated at 30.0 ± 0.1 °C in a constant temperature bath. The concentration of DNA was 200 μM and the flow time was measured with a digital stopwatch, at different loadings of **L** and **1–3** (0–160 μM). Flow time of each sample was tested three times and an average flow time was used. The relative specific viscosity for DNA was calculated using the equation $\eta = (t - t_0)/t_0$, where t and t_0 are the observed flow time for each sample and buffer, respectively. The values of the relative viscosity $(\eta/\eta_o)^{1/3}$ were plotted against binding ratio ($1/R$ = [Compound]/[DNA]).

2.6. *DNA cleaving studies*

The cleavage of SC pUC19 DNA by **L** and **1–3** was monitored by agarose gel electrophoresis under illuminated conditions. SC pUC19 DNA (40 μM) in 50 mM Tris–HCl buffer/50 mM NaCl (pH 7.2) was treated with **L** and **1–3** (20 μM). The chemical nuclease reactions were also carried out in the presence of ascorbic acid (20–100 μM). Dilutions were made with the buffer to a total volume of 20 μL in a dark chamber. After 1 h of incubation at 37 °C, 3 μL loading buffer containing 25% bromophenol blue and 40% sucrose was added to each sample and loaded on 0.8% agarose gel containing 1.0 μg mL^{-1} ethidium bromide. Electrophoresis was carried out at 50 V for 2 h in Tris-boric acid-EDTA (TBE) buffer. The extent of cleavage was calculated from the intensities of the bands using a Gel Documentation System (LARK). The bands in the agarose gel were visualized by UV light and photographed. The errors in the band intensity range from 3% to 8%.

Downloaded by [Mizoram University] at 14:52 28 December 2015

Downloaded by [Mizoram University] at 14:52 28 December 2015

2.7. *3-(4,5-Dimethylthiazol-2-yl)-2,5-diphenyltetrazolium bromide (MTT) assay*

The ability of **L** and **1–3** to interfere with the growth of MCF-7 cells was determined with the support of MTT (3-(4,5-dimethylthiazol-2-yl)-2,5-diphenyltetrazolium bromide) dye assay. The MCF-7 cells were seeded onto 96-well plates in the medium. The cells were washed twice with phosphate-buffered saline (PBS) and MTT reagent [3-(4,5-dimethylthiazol-2-yl)-2,5-diphenyltetrazolium bromide, a yellow tetrazole] in Dulbecco's modified Eagle medium as invitrogen was added at a final concentration of 5 mg mL^{-1} after 24 h treatment with **L** and **1–3** in 100 and 10 μg mL^{-1} concentrations. Similarly, DMSO (solvent control) and Triton X (positive control) were treated. Cells were incubated at 37 °C for 4 h. At the end of the incubation period, the medium was removed and converted crystals solubilized with DMSO. Absorbance of converted dye was measured at 570 nm. Then the percentage of inhibition was calculated by the following formula:

$$\% \text{ inhibition} = 1 - \left(\frac{\text{Test}}{\text{Control}}\right) \tag{3}$$

3. Results and discussion

The Schiff base (**L**) and its binary (**1**) and mixed ligand complexes (**2** and **3**) are non-hygroscopic and stable at room temperature. **1–3** are soluble in methanol, acetonitrile, DMSO, and DMF. The stoichiometries of the compounds were determined as [CuL(A)] on the basis of elemental and ESI mass analysis (scheme 1) and are confirmed by determining the X-ray crystal structure of **2**. The molar conductance values of **1–3** in DMSO (1×10^{-3} M) at room temperature of 4–9 mho M^{-1} cm^2 revealed that all the complexes are non-electrolytes.

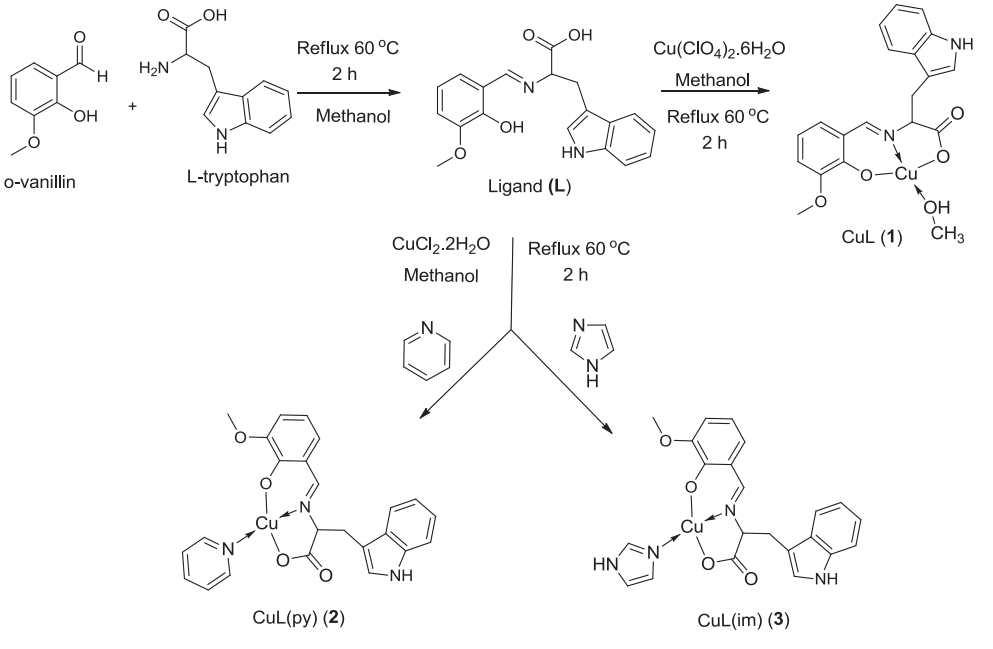

Scheme 1. Synthetic scheme of **L** and its copper complexes (**1–3**).

Downloaded by [Mizoram University] at 14:52 28 December 2015

3.1. *Description of crystal structure of [Cu(L)(NC_6H_5)] (2)*

The ORTEP diagram with atom numbering scheme for **2**, [$C_{25}H_{21}N_3O_5Cu$] is shown in figure 1. Crystallographic data and structure determination parameters are given in table 1. Selected bond lengths and angles of **2** are given in table 2. The X-ray structure analysis shows that the structure consists of monomeric units with the copper center coordinated through N_2O_2 in a distorted square-plane. Out of the four coordination sites, three positions are occupied by imino nitrogen, deprotonated phenolato oxygen, and carboxylato oxygen of the Schiff base. The fourth position of the square plane is occupied by pyridine. The complex crystallized in the triclinic crystal system with P-1 space group. In the complex, all the aromatic rings are planar. The unit cell packing diagram of **2** is given in figure 2. The structure based on the refinement of single crystal data collected shows some disordered solvent molecules in the channels parallel to the *b*-axis. However, refining the structure without solvent molecules resulted in higher *R*-indices [33]. The crystal packing of **2** is stabilized by N–H···O intermolecular hydrogen bonds with N1 a donor to O1/O3 in the molecule (table S1). The ORTEP diagram shows that Cu(1)–O(1) and Cu(1)–O(2) bonds are *trans* and the distances are 1.9630(15) and 1.8951(17) Å, respectively. The slight distortion of the coordination plane can be quantified by measuring the *trans* angles, that are ideally 180° for a square-planar complex. The bond angle of O(1)–Cu(1)–O(2) is 169.48(7)° showing an angular deviation of 10.52° from an exact *trans* coordination. Similarly, Cu–N bonds are in *trans* configuration and the bond distance 2.009(2) Å is for Cu(1)–N(2) and 1.9317(17) Å

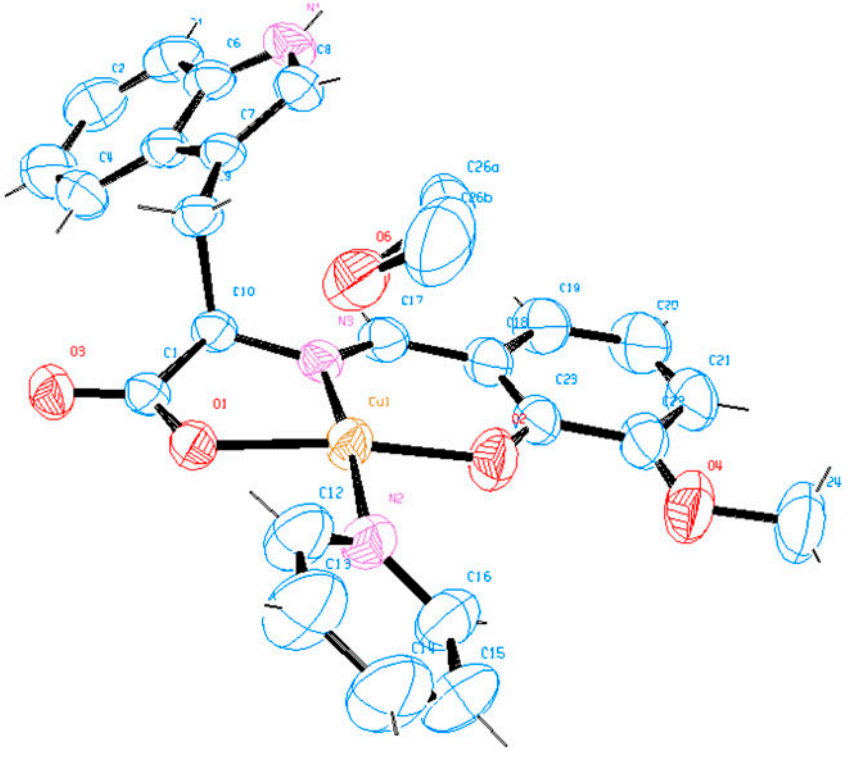

Figure 1. ORTEP view (50% probability level) of the molecular structure of [Cu(L)(pyridine)].

Downloaded by [Mizoram University] at 14:52 28 December 2015

Table 1. Crystallographic data and data collection parameters for **2**.

CCDC	968941
Empirical formula	$C_{25}H_{21}CuN_3O_5$
Formula weight	506.99
Temperature	296(2) K
Wavelength	0.71073 Å
Crystal system, space group	Triclinic, P-1
Unit cell dimensions	a = 9.4063(5) Å, α = 105.597(2)° b = 11.8735(7) Å, β = 106.245(2)° c = 11.9217(7) Å, γ = 96.468(2)°
Volume	1205.57(12) $Å^3$
Z, Calculated density	2, 1.397 Mg m^{-3}
Absorption coefficient	0.946 mm^{-1}
F(0 0 0)	522
Crystal size	0.40 × 0.35 × 0.25 mm
Theta range for data collection	1.82 to 28.21°
Limiting indices	$-12 \le h \le 11$, $-14 \le k \le 15$, $-15 \le l \le 15$
Reflections collected/unique	10,659/5759 [R(int) = 0.0189]
Completeness to theta = 28.21	97.10%
Absorption correction	Semi-empirical from equivalents
Max. and min. transmission	0.7979 and 0.7035
Refinement method	Full-matrix least-squares on F^2
Data/restraints/parameters	5759/0/321
Goodness-of-fit on F^2	1.002
Final R indices [$I > 2\sigma(I)$]	R_1 = 0.0378, wR_2 = 0.1079
R indices (all data)	R_1 = 0.0538, wR_2 = 0.1265
Largest diff. peak and hole	0.505 and −0.383 e·$Å^{-3}$

Table 2. Selected bond lengths (Å) and angles (°) for **2**.

Bond distances	
N(2)–Cu(1)	2.009(2)
N(3)–Cu(1)	1.9317(17)
O(1)–Cu(1)	1.9630(15)
O(2)–Cu(1)	1.8951(17)
Bond angles	
O(2)–Cu(1)–N(3)	93.59(8)
O(2)–Cu(1)–O(1)	169.48(7)
N(3)–Cu(1)–O(1)	83.69(7)
O(2)–Cu(1)–N(2)	90.24(8)
N(3)–Cu(1)–N(2)	174.92(8)
O(1)–Cu(1)–N(2)	91.94(7)
C(16)–N(2)–Cu(1)	121.6(2)
C(17)–N(3)–Cu(1)	126.38(16)
C(10)–N(3)–Cu(1)	113.70(12)
C(11)–O(1)–Cu(1)	115.19(12)
C(23)–O(2)–Cu(1)	126.79(17)
C(17)–N(3)–C(10)	119.85(19)
C(22)–O(4)–C(24)	118.2(3)

corresponding to Cu(1)–N(3) bond. The bond angle of N(2)–Cu(1)–N(3) is 174.92(8)°. The O(2)–Cu(1)–N(2) and O(1)–Cu(1)–N(2) bond angles are 90.24(8)° and 91.94(7)°, respectively, and these values are similar to the values reported for Cu(II) complexes with N_2O_2 donors [34]. Overall, the bond lengths and angles of **2** are in close agreement with those reported for other mixed ligand copper(II) complexes [35, 36].

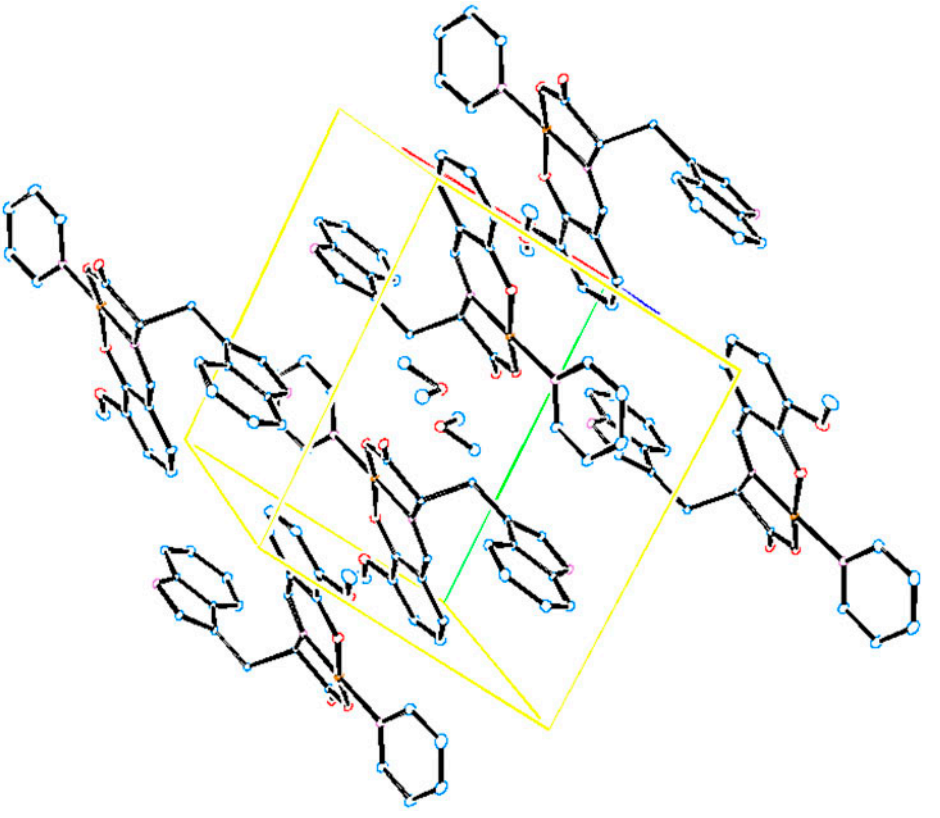

Figure 2. Crystal packing diagram of **2**.

3.2. *IR-spectra*

The formation of amino acid Schiff base by condensation of L-tryptophan and *o*-vanillin is shown from the azomethine group (–CH=N–) absorption at 1635 cm^{-1}. This band shifted to lower wavenumber (1621–1626 cm^{-1}) in the complexes suggesting that the azomethine nitrogen is coordinated with copper. The ν(NH) indole peak of **L** did not show a noticeable shift during complexation, indicating non-involvement of indole -NH in coordination with copper. **L** shows bands at 1612 and 1394 cm^{-1} attributed to $\nu(COO^{-})_{asym}$ and $\nu(COO^{-})_{sym}$ of carboxylate, respectively. These bands are shifted to lower values (1604 and 1384 cm^{-1}) in complexes. The magnitude of separation between these two vibrations of 248–254 cm^{-1} suggests the unidentate coordination of carboxylate [37]. In all the complexes, the phenolic $\nu_{(C-O)}$ band of **L** at 1226 cm^{-1} is shifted to lower frequency (1216–1219 cm^{-1}), indicating coordination of the deprotonated phenolic oxygen to copper. The presence of pyridine in **2** is confirmed by the observation of highly distressed in-plane-ring bending and out-of-plane-ring bending bands at 1534, 698, and 534 cm^{-1}. In **3**, $\nu_{(C=N)}$ vibration of imidazole ring (1678 cm^{-1}) is shifted by 26 cm^{-1}, indicating coordination of imidazole nitrogen to copper ion. The bands at 550–555 cm^{-1} and 426–434 cm^{-1} are assigned to $\nu_{(Cu-N)}$ and $\nu_{(Cu-O)}$ stretches, respectively.

Downloaded by [Mizoram University] at 14:52 28 December 2015

Downloaded by [Mizoram University] at 14:52 28 December 2015

3.3. *Mass spectra*

Metal ligand stoichiometries are shown by comparison of ESI mass spectroscopy of ligand and its copper complexes (figure S2). **L** shows the molecular ion peak $[M + H]^+$ at $m/z = 339$ (100%), which is equal to its molecular mass. Complex **1** shows a molecular ion peak at $m/z = 441$, which corresponds to the solvated (coordinated acetonitrile) complex. In the analytical report, the complex contains a coordinated methanol. By recording ESI mass spectrum of **1** in acetonitrile, methanol is replaced with acetonitrile. The solvent-free complex is detected at m/z 400. Complex **2** in acetonitrile shows molecular ion peak at 479.1 m/z demonstrating that pyridine is coordinated with Cu(II). The mass spectrum of **3** in acetonitrile gives peak at 468 (100%), indicating the presence of imidazole in **3**. The fragmentation peaks of **3** show the presence of solvated (coordinated acetonitrile, $m/z = 440.65$) and solvent-free ($m/z = 400$) complexes. The dimer of the compounds is also observed in the corresponding spectra. The molecular ion and fragmentation peaks of the complexes have half intensity peaks due to isotopic distributions of copper (^{63}Cu and ^{65}Cu) [38]. The mass spectra of the ligand and its copper complexes are in agreement with their proposed structure. The m/z values of molecular ions and fragmentation species of **L**, **1**, **2,** and **3** are given in table S2.

3.4. *Electronic spectra*

The electronic spectra of **L** and **1–3** were recorded in DMSO (figure 3). **L** shows bands at 293 nm ($\varepsilon_{max} = 6925\ M^{-1}\ cm^{-1}$) and 422 nm ($\varepsilon_{max} = 3370\ M^{-1}\ cm^{-1}$). The band at 293 nm is attributed to the π–π^* transition of hetero-aromatic moiety. The band at 422 nm corresponds to π–π^* transition of azomethine chromophore which undergoes a hypsochromic shift during complexation, indicating that **L** forms a complex with copper. The three spin-allowed transitions expected for square-planar complexes with a $d_{x^2-y^2}$ ground state viz. $^2B_{1g} \rightarrow {}^2B_{2g}(d_{x^2-y^2} \rightarrow d_{xy})$, $^2B_{1g} \rightarrow {}^2A_{2g}(d_{x^2-y^2} \rightarrow d_{z^2})$ and $^2B_{1g} \rightarrow {}^2E_g(d_{x^2-y^2} \rightarrow d_{xz,yz})$, which

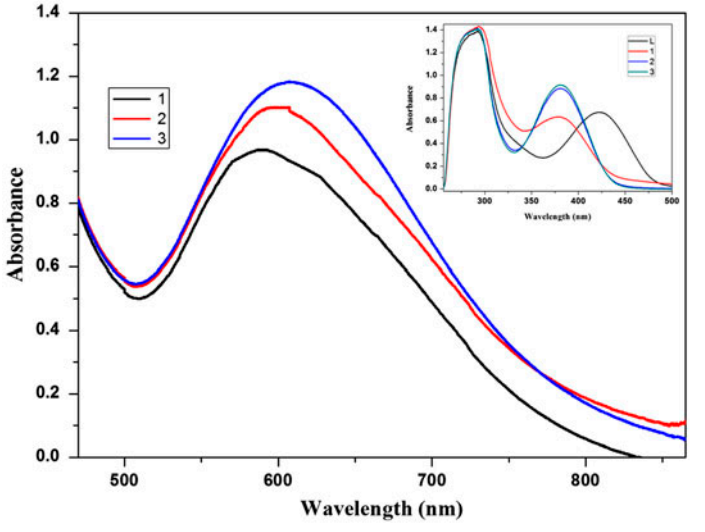

Figure 3. Electronic spectra of **1–3** in DMSO in the visible region. Inset: electronic spectra of **L** and **1–3** in UV region.

are very close in energy appear as a broad absorption around 600 nm. The d–d transitions of **1**, **2,** and **3** observed, respectively, at 590, 598, and 607 nm are consistent with a distorted square-planar structure [39, 40].

3.5. *Electron paramagnetic resonance spectra*

The X-band EPR spectra of **1–3** were recorded in DMSO at room and liquid nitrogen temperature (figure 4). The spectra in frozen solution show four well-resolved peaks of low intensities in the low-field region and one intense peak in the high-field region resulting from the coupling of the unpaired electron with the nuclear spin of Cu(II). The $g_{\|}$ and $g_{\perp}$ values ($g_{\|} > g_{\perp} > g_e$) and G values [$G = (g_{\|} - g_e)/(g_{\perp} - g_e)$] indicate that the unpaired electron is in $d_{x^2-y^2}$ orbital of Cu(II) ($^2B_{1g}$ as the ground state) in square-based geometries [41] (table 3). The G values observed for the complexes (G = 5.4–5.7) suggest that the exchange coupling effects are not operative in the present complexes. The $g_{\|} > g_{\perp}$ accounts for the distorted square-planar structure and rules out the possibility of a trigonal bipyramidal structure, which would be expected to have $g_{\|} > g_{\perp}$ [42]. The empirical ratio ($g_{\|}/A_{\|}$) expected for a square-planar Cu(II) complex ranges from 105 to 135 cm^{-1} [43]. In the present investigation, the $g_{\|}/A_{\|}$ values for **1–3** are 118–132 cm^{-1}, within the range expected for a square-planar Cu(II) coordination geometry.

3.6. *Electrochemical investigation*

Electrochemical behaviors of **L** and **1–3** were studied using cyclic voltammetry in the potential range –1.0 to +1.5 V *versus* Ag/AgCl. Cyclic voltammogram (100 mV s^{-1}) of **L** shows a peak at 0.700 V that is shifted to positive potential in **1–3**, indicating the complexation of **L** with copper. A typical voltammogram of **1** is displayed in figure S3. At lower

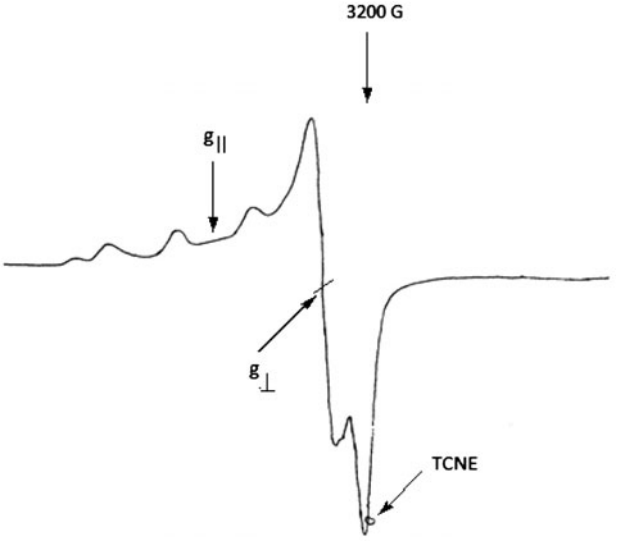

Figure 4. X-band EPR spectrum of **1** at liquid nitrogen temperature with TCNE as a standard.

Downloaded by [Mizoram University] at 14:52 28 December 2015

Table 3. Electronic and EPR spectral data of **1–3**.

Complex	λ_{max}, nm (ε, M^{-1} cm^{-1})			Hyperfine constant				
				$A_{\parallel} \times 10^{-4}$ cm^{-1}	$g_{\parallel}$	$g_{\perp}$	$g_{\parallel}/A_{\parallel}$ cm	G
1	293(7185)	380(3190)	590(84.86)	173	2.296	2.056	132	5.693
2	298(6870)	381(4445)	598(117.20)	189	2.276	2.052	120	5.426
3	293(6995)	381(4574)	607(117.77)	190	2.252	2.048	118	5.551

scan rate (50 mV s^{-1}), the complexes show a cathodic peak that ranges from 0.020 to 0.0245 V attributed to Cu(II) → Cu(I) and the corresponding oxidation peak Cu(I) to Cu(II) appears in the range 0.245 to 0.257 V. The complexes display a weak peak at –0.340 to –0.355 V due to Cu(I) → Cu(0) reduction, and the corresponding oxidation peaks are not observed. At higher scan rate (250 mV s^{-1}), a weak peak at –0.22 V corresponds to Cu(0) → Cu(I) oxidation. Also, the peak current of Cu(I) → Cu(II) and Cu(I) → Cu(0) processes are enhanced. From these experimental results, it is evident that the formation of Cu(I) species in this electrochemical mechanism has a short lifetime which could not be detected at lower scan rate [44]. The complexes exhibit higher reduction potential for Cu(II) → Cu(I) and Cu(I) → Cu(0) compared to free copper ion [usually the reduction potentials are –0.6 to –0.9 V *versus* Ag/AgCl] [45]. This indicates that the ligand possesses unsaturated nitrogens which delocalize the electron around the ligand system and thus facilitate the reduction process.

3.7. *DNA binding studies*

3.7.1. Absorption spectral studies. The DNA binding abilities of **L** and its complexes were studied by electronic absorption titration. The typical titration curves for **L** and **1–3** are shown in figure 5 and the results are reported in table 4. **L** shows absorptions at 267 and 343 nm in Tris–HCl buffer solution from π–π^* transition of hetero-aromatic moiety and π–π^* transition of azomethine chromophore, respectively. With the addition of DNA, **L** exhibits a small increase (3 nm) in the wavelength and intensity of the absorption band [figure 5(a)]. In **L**, the indole –NH at position 1 is a potent H-bond donor. The side chain attached to the indole ring contains strong H-bond acceptor (–C=N) and H-bond donor (–COOH) groups. The H-bond donor or acceptor groups of **L** may form one or two H-bonds during their interaction with DNA duplex in its minor groove. It is evident from the perturbation (increases in the λ_{max} and the hyperchromicity) observed in the electronic spectrum of **L** with the addition of DNA. The charge transfer band for **1**, **2,** and **3** in buffer solution is observed at 362, 370, and 360 nm, respectively. Upon increasing the CT-DNA concentration, hyperchromism is observed for the copper complexes [figure 5(b)–(d)]. However, there is no change in the position of the absorption suggesting groove binding between copper complex and DNA. The minor groove contains primarily H-bond acceptor groups, the purine N(3), and pyrimidine O(2) at the floor of the groove walls [46]. The indole ring of the copper complexes contains an uncoordinated –NH–, which may involve H-bonding with DNA. The K_b values determined for **L**, **1**, **2,** and **3** agree well with the binding constant values reported for copper complexes involved in binding with CT-DNA [47–54]. The intrinsic binding constant K_b is **L** < **1** < **2** < **3**. The binding constants (K_b) for **L** and **1–3** (table 4) are lower than classical intercalators (*e.g.*, EB-DNA, ~10^6 M^{-1}) [55], but higher than those of some non-intercalating copper(II) complexes [56].

Downloaded by [Mizoram University] at 14:52 28 December 2015

Downloaded by [Mizoram University] at 14:52 28 December 2015

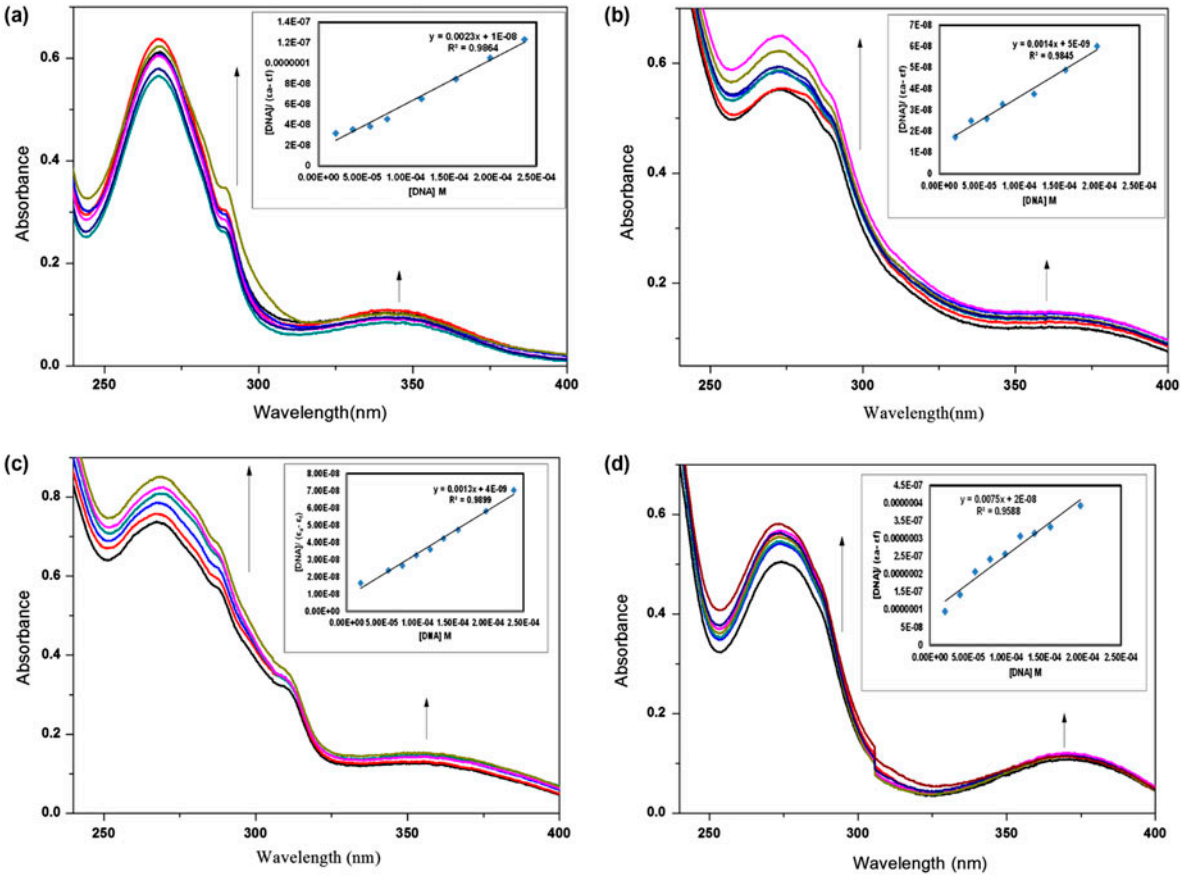

Figure 5. Electronic spectra of (a)**L**, (b)**1**, (c)**2,** and (d)**3** in Tris–HCl buffer upon addition of calf-thymus DNA. [Compound] = 20 μM, [DNA] = 0–120 μM. Arrow shows the absorption intensities changes upon increasing DNA concentration. Inset: plots of $[DNA]/(\varepsilon_a - \varepsilon_f)$ *vs.* [DNA] for titration of **L**, **1**, **2,** and **3** with CT-DNA.

Table 4. Absorption and emission spectral properties of **L** and **1–3** with CT-DNA.

Compound	Electronic spectra			Fluorescence spectra		
	λ_{max} (nm)	Change in absorption	K_b (M^{-1})	λ_{max} (nm)	K_{app} (M^{-1})	K_{SV} (M^{-1})
L	267, 343	Hyperchromism	2.3×10^5	615	–	–
1	273, 362	Hyperchromism	2.8×10^5	615	6.0×10^5	1.01×10^4
2	269, 370	Hyperchromism	3.3×10^5	615	5.5×10^5	1.29×10^4
3	274, 360	Hyperchromism	3.8×10^5	615	5.0×10^5	2.07×10^4

3.7.2. Fluorescence studies (competitive binding studies). The competitive binding of **1–3** with ethidium bromide (EB) were investigated with fluorescence displacement experiments. The conjugate planar EB has weak fluorescence intensity in Tris–HCl buffer. But, the fluorescence intensity of EB is greatly increased when intercalated into base pairs of double-stranded DNA. The additions of **1–3** to EB-DNA adduct causes appreciable reduction in the emission intensity, indicating that these compounds competitively bind to CT-DNA. The emission spectra of the EB-DNA adduct in the absence and presence of **1–3** are given in figure 6. Intercalators and groove binders can quench the emission of DNA-bound EB by replacing EB and/or by accepting the excited state electron of EB through a photo-electron transfer mechanism [57]. Increasing concentrations of **1**, **2,** and **3** to EB-DNA causes a reduction in emission intensity of *ca.* 35%, 40%, and 42%, respectively. This quenching is due to accepting the excited state electron of EB through a photo-electron transfer mechanism. The quenching constants (K_{SV}) calculated from the Stern–Volmer plots (table 4) indicate that the quenching efficiency of **3** is higher than those of other compounds. The apparent binding constants (K_{app}) determined from fluorescence studies are consistent with the binding constants (K_b) of the absorption titration studies, suggesting that these compounds bind to CT-DNA through minor groove binding. The association constants (K_{app}) of **1–3**, 6.0×10^5, 5.5×10^5, and 5.0×10^5 M^{-1}, agree well with binding constants reported for copper complexes with CT-DNA [56].

3.7.3. Viscosity measurement. Viscosity measurement is essential analysis of binding mode of DNA in solution. Viscosity parameter is important as it is sensitive to change in length of the DNA strands upon binding with metal complexes. Compound binding with DNA through intercalation results in lengthening of DNA, producing an increase in the relative specific viscosity of solution of DNA. In contrast, partial and/or non-classical intercalation (grooves) with the DNA helix result in a decrease in its effective length with minor changes in the viscosity [58]. On increasing the amount of compounds (**L**, **1**, **2,** and **3**) to CT-DNA, less pronounced effect observed on the relative viscosity of DNA (figure 7) suggests groove binding between compounds and DNA.

3.8. *Chemical nuclease activity*

The DNA cleaving ability of **L** and **1–3** was tested against supercoiled plasmid pUC19 DNA by electrophoresis in Tris–HCl buffer medium. The plasmid DNA was subjected with **L** and **1–3** for an hour at 37 °C leading to cleavage of supercoiled (SC) form to nicked (NC) form (figure 8). **L** and **1–3** show DNA cleavage activity even in the absence of any external reagent. Complex **3** produces 85% of NC form and rest of the compounds (**L**, **1,** and **2**) show 30–35% cleavage activity against the DNA (table S3). The cleavage activity of

Downloaded by [Mizoram University] at 14:52 28 December 2015

Downloaded by [Mizoram University] at 14:52 28 December 2015

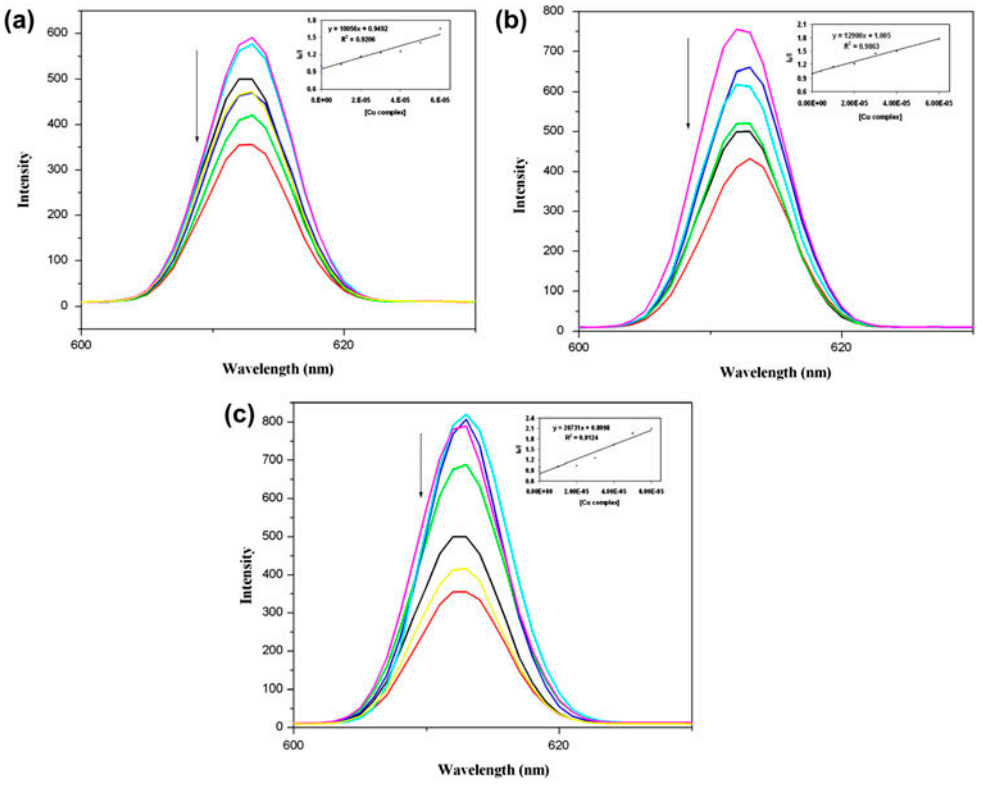

Figure 6. Fluorescence spectra of EB (2.5 μM) with CT-DNA (10 μM) in the absence and presence of increasing amount of compounds (0–60 μM); (a) **1**, (b) **2,** and (c) **3**. Arrow shows the intensity change upon increasing concentration of compounds. The red line represents the emission spectrum of EB in the absence of DNA in Tris–HCl buffer (see http://dx.doi.org/10.1080/00958972.2015.1008466 for color version).

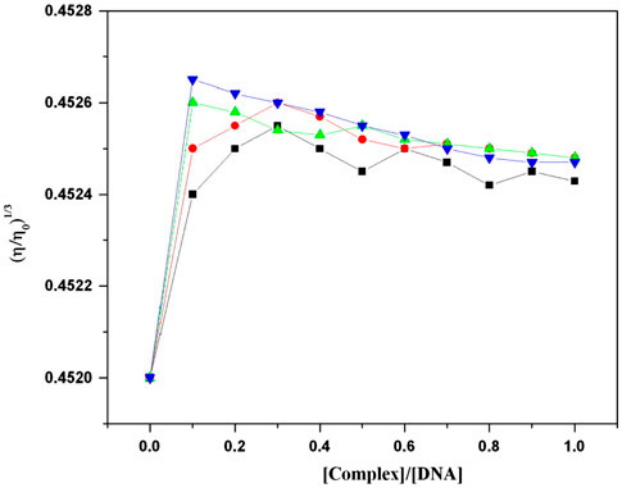

Figure 7. Change in relative specific viscosity of CT-DNA (200 μM) on addition of **L** (●), **1** (▲), **2** (■), and **3** (▼) (0–160 μM) in Tris–HCl buffer (pH 7.2) at 37 °C.

the compounds may be due to secondary interaction of indole –NH with DNA bases. In addition to indole –NH interaction, **3** has uncoordinated imidazole –NH which involves secondary interactions like H-bonding with DNA leading to higher DNA cleavage activity. Thus, **1–3** are able to cleave DNA in the absence of external reagent (oxidizing or reducing agent), completely ruling out the possibility of an oxidative cleavage mechanism. In the presence of ascorbic acid as an activator, **L** shows less effect and the complexes show higher activity [**2** (100%) > **3** (97%) > **1** (70%)]. These results suggest that **1–3** produce active species (·OH) by the reduction of DNA-bound complexes by ascorbic acid and are subjected to the one-electron oxidation by hydrogen peroxide. The generated ·OH are responsible for the DNA cleavage and the possible course of events is as follows,

$$\text{Ascorbate} + O_2 \rightarrow \text{Dehydroascorbate} + H_2O_2$$

$$\text{Ascorbate} + 2Cu^{2+} \rightarrow \text{Dehydroascorbate} + 2Cu^{+}$$

$$Cu^{+} + H_2O_2 \rightarrow Cu^{2+} + {}^{\cdot}OH + OH^{-}$$

3.9. *MTT assay*

Cell death by damaging DNA is essential for a drug to act as an anticancer agent. Metal containing drugs cause cross linking of DNA by interfering with cell division, which in turn activates apoptosis. **L** and **1–3** have the ability to bind strongly with DNA and cleave the DNA in the absence, as well as in the presence, of a reductant. Hence, we have carried out *in vitro* assays to evaluate the cytotoxic effects of **L** and **1–3** against human breast cancer cell lines (MCF-7) (figure 9). From the percentage of inhibition, all the complexes (**1–3**) exhibit significant activity against MCF-7 cells compared to **L**. Cytotoxicity of the complexes was compared with that of cisplatin. The percentage inhibition of cisplatin

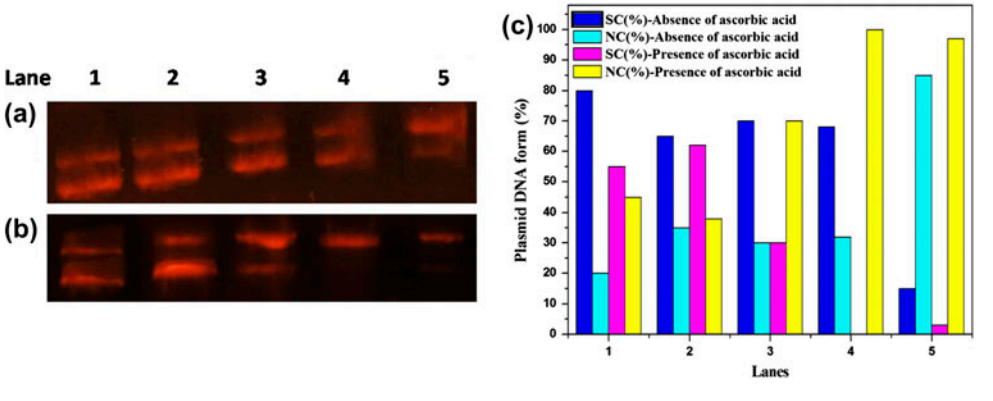

Figure 8. Cleavage of SC pUC19 DNA (40 μM) by **L** and complexes (20 μM); (a) in the absence of ascorbic acid, (b) in the presence of ascorbic acid. Lane 1: DNA control; Lane 2: DNA + **L**; Lane 3: DNA + **1**; Lane 4: DNA + **2**; Lane 5: DNA + **3**, and (c) Relative amounts of the different DNA forms (%) Lanes 1–5; Control DNA, DNA + **L**, DNA + **1**, DNA + **2**, DNA + **3**.

Downloaded by [Mizoram University] at 14:52 28 December 2015

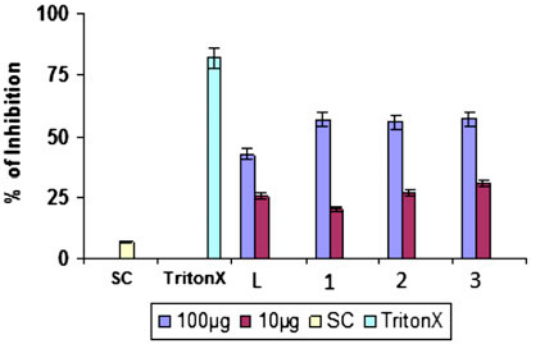

Figure 9. Effect of **L** and its copper complexes (**1–3**) on the inhibition of breast cancer cells.

(20 µg) against MCF-7 cell is more than 98% [59]. The Cu(II) complexes (**1–3**) (10 µg) exhibit 63% inhibition against MCF-7 cells, indicating the possibility of specific toxicity to cancer cells.

4. Conclusion

Binary and mixed ligand Cu(II) complexes containing amino acid Schiff base and heterocyclic nitrogen co-ligands, imidazole, and pyridine were studied. The Cu(II) complex containing pyridine (**2**) has been structurally characterized by X-ray crystallography and shows triclinic crystal system with N_2O_2 coordination sphere. Electrochemical studies reveal that the unsaturated nitrogen of the ligand delocalizes the electrons around the ligand system and facilitate reduction in metal complexes. This work provides insight into the binding and cleaving nature of the complexes with DNA. The complexes interact with DNA through groove binding and follow the order: **L** < **1** < **2** < **3**. The chemical nuclease activity of the complexes to SC pUC19 DNA in the absence of any external reagent rules out the possibility of an oxidative cleavage mechanism. The *in vitro* cytotoxicity of the complexes tested against breast cancer cell lines (MCF-7) exhibit potential cytotoxic effects.

Supplementary material

Spectra, DNA binding activity, and cyclic voltammogram are embedded in the supplementary materials. CCDC 968941 contains the crystallographic data for **2**. These data can be obtained free of charge via http://www.ccdc.cam.ac.uk/conts/retrieving.html or from the Cambridge Crystallographic Data Center, 12 Union Road, Cambridge CB2 1EZ, UK; Fax: + 44 1223 336 033; or E-mail: deposit@ccdc.cam.ac.uk.

Acknowledgements

Council of Scientific and Industrial Research (CSIR), New Delhi, India [01(2736)/13/EMR-II] is gratefully acknowledged for financial support. One of the authors (C.B.) thanks CSIR for

Downloaded by [Mizoram University] at 14:52 28 December 2015

the fellowship. We thank Dr B.S. Lakshmi, Centre for Biotechnology, Anna University, Chennai for cytotoxicity studies. Authors thank SAIF, Mumbai for EPR spectra and STIC, Cochin for single crystal XRD and NMR spectra.

References

[1] K.H. Thompson, C. Orvig. *Science*, **300**, 936 (2003).
[2] A.M. Pyle, J.K. Barton, S.J. Lippard. *Prog. Inorg. Chem.*, **38**, 413 (1990).
[3] J.J.R. Frausto da Silva, R.J.P. Williams. *The Biological Chemistry of the Elements: The Inorganic Chemistry of Life*, 2nd Edn, Oxford University Press, Oxford (2001).
[4] V.M. Manikandamathavan, T. Weyhermuller, R.P. Parameswari, M. Sathishkumar, V. Subramanian, B.U. Nair. *Dalton Trans.*, **43**, 13018 (2014).
[5] A.K. Patra, T. Bhowmick, S. Roy, S. Ramakumar, A.R. Chakravarty. *Inorg. Chem.*, **48**, 2932 (2009).
[6] Q. Wang, Z.Y. Yang, G.F. Qi, D.D. Qin. *Eur. J. Med. Chem.*, **44**, 2425 (2009).
[7] B. Bektasoglu, S.E. Celik, M. Ozyurek, K. Guclu, R. Apak. *Biochem. Biophys. Res. Commun.*, **345**, 1194 (2006).
[8] B. Lippert. *Cisplatin: Chemistry and Biochemistry of a Leading Anticancer Drug*, p. 563, Verlag Helvetica Chimica Acta, Zurich (1999).
[9] P.J. Bednarski, F.S. Mackay, P.J. Sadler. *Anticancer Agents Med. Chem.*, **7**, 75 (2007).
[10] H.T. Chifotides, K.R. Dunbar. *Acc. Chem. Res.*, **38**, 146 (2005).
[11] Y.Y. Kou, J.L. Tian, D.D. Li, H. Liu, W. Gu, S.P. Yan. *J. Coord. Chem.*, **62**, 2182 (2009).
[12] S. Rajalakshmi, T. Weyhermüller, M. Dinesh, B.U. Nair. *J. Inorg. Biochem.*, **117**, 48 (2012).
[13] M.L. Liu, M. Jiang, K. Zheng, Y.T. Li, Z.Y. Wu, C.W. Yan. *J. Coord. Chem.*, **67**, 630 (2014).
[14] M. Iqbal, S. Ali, Z.U. Rehman, N. Muhammad, M. Sohail, V. Pandarinathan. *J. Coord. Chem.*, **67**, 1731 (2014).
[15] R.C. Santra, K. Sengupta, R. Dey, T. Shireen, P. Das, P.S. Guin, K. Mukhopadhyay, S. Das. *J. Coord. Chem.*, **67**, 265 (2014).
[16] C. Rajarajeswari, R. Loganathan, M. Palaniandavar, E. Suresh, A. Riyasdeen, M.A. Akbarsha. *Dalton Trans.*, 8347 (2013).
[17] Z.B. Ou, Y.H. Lu, Y.M. Lu, S. Chen, Y.H. Xiong, X.H. Zhou, Z.W. Mao, X.Y. Le. *J. Coord. Chem.*, **66**, 2152 (2013).
[18] S. Thalamuthu, B. Annaraj, S. Vasudevan, S. Sengupta, M.A. Neelakantan. *J. Coord. Chem.*, **66**, 1805 (2013).
[19] S. Thalamuthu, B. Annaraj, M.A. Neelakantan. , *Spectrochim. Acta, Part A*, **118**, 120 (2014).
[20] C. Gao, X. Ma, J. Lu, Z. Wang, J. Tian, S. Yan. *J. Coord. Chem.*, **64**, 2157 (2011).
[21] P.R. Reddy, A. Shilpa, N. Raju, P. Raghavaiah. *J. Inorg. Biochem.*, **105**, 1603 (2011).
[22] S. Ramakrishnan, D. Shakthipriya, E. Suresh, V.S. Periasamy, M.A. Akbarsha, M. Palaniandavar. *Inorg. Chem.*, **50**, 6458 (2011).
[23] S. Ramakrishnan, V. Rajendiran, M. Palaniandavar, V.S. Periasamay, B.S. Srinag, H. Krishnamurthy, M.A. Akbarsha. *Inorg. Chem.*, **48**, 1309 (2009).
[24] M.A. Neelakantan, M. Sundaram, M.S. Nair. *Spectrochim. Acta, Part A*, **79**, 1693 (2011).
[25] M.A. Neelakantan, S.S. Mariappan, J. Dharmaraja, K. Muthukumaran. *Acta Chim. Slovenica*, **57**, 198 (2010).
[26] M.A. Neelakantan, M. Sundaram, M.S. Nair. *J. Chem. Eng. Data*, **56**, 2527 (2011).
[27] A.I. Vogel. *Text Book of Practical Organic Chemistry*, 5th Edn, Longman, London (1989).
[28] Bruker. *APEX2, SAINT and SADABS*, Bruker AXS Inc., Madison, WI (2008).
[29] G.M. Sheldrick, SHELXS-97 and SHELXL-97. *Program for the Solution of Crystal Structures*, University of Gottingen, Germany (1997).
[30] M. Nardelli. *J. Appl. Crystallogr.*, **28**, 659 (1995).
[31] A. Wolfe, G.H. Shimer, T. Meehan. *Biochemistry*, **26**, 6392 (1987).
[32] O. Stern, M. Volmer. *Phys. Z.*, **20**, 183 (1919).
[33] D. Poleti, L. Karanovic, A. Kremenovic, J. Rogan. *J. Serb. Chem. Soc.*, **72**, 767 (2007).
[34] S.M. Haidad Ali, Y.K. Yan, P.P.F. Lee, K.Z.X. Khong, M. Alam Sk, K.H. Lim, B. Klejevskaja, R. Vilar. Dalton Trans., 1449 (2014).
[35] L.L. Koh, J.O. Ranford, W.T. Robinson, J.O. Svensson, A.L. Choo Tan, D. Wu. *Inorg. Chem.*, **35**, 6466 (1996).
[36] R.N. Patel, N. Singh, V.L.N. Gundla. *Polyhedron*, **25**, 3312 (2006).
[37] K. Nakamoto. *Infrared and Raman Spectra of Inorganic and Coordination Compounds, Part A: Theory and Applications in Inorganic Chemistry*, 5th Edn, Wiley, New York (1997).
[38] A. Matsumoto, T. Fukumoto, H. Adachi, H. Watarai. *Anal. Chim. Acta*, **390**, 193 (1999).
[39] C.C. Su, S.Y. Chiu. *Polyhedron*, **15**, 2623 (1996).
[40] V. Selvarani, B. Annaraj, M.A. Neelakantan, S. Sundaramoorthy, D. Velmurugan. *Polyhedron*, **54**, 74 (2013).
[41] B.J. Hathaway, D.E. Billing. *Coord. Chem. Rev.*, **5**, 143 (1970).

Downloaded by [Mizoram University] at 14:52 28 December 2015

[42] M. Murali, M. Palaniandavar, T. Pandiyan. *Inorg. Chim. Acta*, **224**, 19 (1994).
[43] U. Sakaguchi, A.W. Addison. *J. Chem. Soc., Dalton Trans.*, 600, (1979).
[44] D.K. Gosser. *Cyclic Voltammetry: Simulation and Analysis of Reaction Mechanisms*, VCH, New York (1993).
[45] P. Zanello. *Inorganic Electrochemistry Theory, Practice and Application*, Royal Chemical Society, Cambridge (2003).
[46] S. Rajalakshmi, T. Weyhermuller, A.J. Freddy, H.R. Vasanthi, B.U. Nair. *Eur. J. Med. Chem.*, **46**, 608 (2011).
[47] L. Shiva Kumar, H.D. Revanasiddappa. *J. Coord. Chem*., 64, 699 (2011).
[48] S.P. Devi, R.K.B. Devi, M. Damayanti, N.R. Singh, R.K.H. Singh, R.M. Kadam. *J. Coord. Chem.*, **64**, 1586 (2011).
[49] H.H. Lu, Y.T. Li, Z.Y. Wu, K. Zheng, C.W. Yan. *J. Coord. Chem.*, **64**, 1360 (2011).
[50] X.L. Wang, M. Jiang, Y.T. Li, Z.Y. Wu, C.W. Yan. *J. Coord. Chem.*, **66**, 1985 (2013).
[51] X.W. Li, M. Jiang, Y.T. Li, Z.Y. Wu, C.W. Yan. *J. Coord. Chem.*, **63**, 1582 (2010).
[52] S.H. Cui, M. Jiang, Y.T. Li, Z.Y. Wu, X.W. Li. *J. Coord. Chem.*, **64**, 4209 (2011).
[53] Y. Mei, J.J. Zhou, H. Zhou, Z.Q. Pan. *J. Coord. Chem.*, **65**, 643 (2012).
[54] S. Ramakrishnan, E. Suresh, A. Riyasdeen, M.A. Akbarsha, M. Palaniandavar. *Dalton Trans.*, 3524 (2011).
[55] G.D. Storrier, S.B. Colbran, D.C. Craig. *J. Chem. Soc., Dalton Trans*., 3011 (1997).
[56] R.K.B. Devi, S.P. Devi, R.K.B. Singh, R.K.H. Singh, T. Swu, W.R. Devi, C.H.B. Singh. *J. Coord. Chem.*, **67**, 891 (2014).
[57] J.K. Barton, J.M. Goldberg, C.V. Kumar, N.J. Turro. *J. Am. Chem. Soc.*, **108**, 2081 (1986).
[58] E.J. Gabbay, R.E. Scofield, C.S. Baxter. *J. Am. Chem. Soc.*, **95**, 7850 (1973).
[59] C.W. Yde, M.G. Hansen, A.E. Lykkesfeldt, O.G. Issinger, J. Stenvang. *Mol. Cancer Ther.*, **6**, 1869 (2007).

Downloaded by [Mizoram University] at 14:52 28 December 2015